



The effect of molecular structure on the efficiency of 1,4-diazine-based D-(π)-A push-pull systems for non-doped OLED applications

Egor V. Verbitskiy^{a,b,*}, Yuriy A. Kvashnin^a, Pavel I. Bogdanov^b, Margarita V. Medvedeva^b, Tatyana S. Svalova^b, Alisa N. Kozitsina^b, Lubov G. Samsonova^c, Konstantin M. Degtyarenko^c, Denis V. Grigoryev^c, Alexander E. Kurtcevich^c, Ruslan M. Gadirov^c, Gennady L. Rusinov^{a,b}, Oleg N. Chupakhin^{a,b}, Valery N. Charushin^{a,b}

^a I. Postovsky Institute of Organic Synthesis, Ural Branch of the Russian Academy of Sciences, S. Kovalevskaya Str., 22, Ekaterinburg, 620108, Russia

^b Ural Federal University, Mira St. 19, Ekaterinburg, 620002, Russia

^c Tomsk State University, Novosobornaya sq. 1, Tomsk, 634050, Russia

ARTICLE INFO

Keywords:

Pyrazine
Quinoxaline
OLEDs
Organic emitter

ABSTRACT

A series of novel D-A and D- π -A push-pull systems based on a pyrazine and quinoxaline acceptor, bearing various electron-donating triphenylamine and carbazole moieties, are compared. A significant difference in electrochemical and photophysical properties was found depending on molecular structure. The compounds have strong solvatochromic properties. Quinoxaline-containing systems exhibit delayed fluorescence (DF) in thermal vacuum deposition films. Despite the low quantum yield of fluorescence in the solid state (less than 10%), organic light-emitting diodes with sufficiently high efficiency (4.2 cd/A) have been fabricated on the basis of this push-pull systems. The best results were obtained for compounds exhibiting DF. The possible channel for increasing the efficiency of OLED can be associated with the "hot excitons" mechanism.

1. Introduction

Organic light-emitting diodes (OLEDs) have attracted increasing interest in both the scientific and commercial fields due to their applications in high-resolution, multicolor displays and solid-state lighting [1–4]. Extensive studies have demonstrated that D-(π)-A structures are useful for developing high-efficiency emitters, because such push-pull systems usually show strong intramolecular charge-transfer (ICT) emission and their optoelectronic properties can be facily modulated through tuning the electron donor (D) and/or acceptor (A) strengths [5, 6].

During recent years, pyrazine and quinoxaline derivatives have been intensively studied because as building blocks of π -conjugated compounds for use in multiple optoelectronic and photovoltaic applications [7–9]. The introduction of 1,4-diazine ring into π -extended systems is a way of modifying and enhancing the useful properties where electron transport is necessary. Pyrazine and quinoxaline themselves are commonly used as an electron-acceptor unit (A) which, being combined with different electron-donor blocks, make up for donor-acceptor type

systems. Such push-pull 1,4-diazine-based structures are promising materials for different photovoltaics and optoelectronics applications like dye-sensitized solar cells (DSSCs), organic field-effect transistors, and emitting material for OLEDs [10–12].

On the other hand, fluorescent organic molecules and polymers bearing π -conjugated triphenylamine or carbazole fragments have gained the attention of both experimental and theoretical chemists. These molecules have found wide applications in organic light-emitting diodes (OLEDs), nonlinear optics, dye-sensitized solar cells, and field-effect transistors (FETs) [13–26]. It is possible because of the broad functionalization possibility that enables control of their properties including charge transport ability, stability, fluorescence activity, and HOMO-LUMO energy levels [27–29].

Besides, the introduction of thiophenes, in turn, leads to rigidification and planarization of the compound framework and hence to increased conjugated length [30,31]. This property in combination with good charge transport ability lead to a variety of semiconducting materials including D- π -A systems in which thiophenes are used as π -conjugated linkers.

* Corresponding author. I. Postovsky Institute of Organic Synthesis, Ural Branch of the Russian Academy of Sciences, S. Kovalevskaya Str., 22, Ekaterinburg, 620108, Russia.

E-mail address: verbitskye@yandex.ru (E.V. Verbitskiy).

<https://doi.org/10.1016/j.dyepig.2020.109124>

Received 13 August 2020; Received in revised form 23 December 2020; Accepted 23 December 2020

Available online 30 December 2020

0143-7208/© 2020 Elsevier Ltd. All rights reserved.

The modification of the push-pull system by introducing additional π -conjugated linker makes the final properties of the materials depend on chemical structures of the D and A. The main role of the π -linker is to facilitate and elongate the π -conjugation chain between the donor and acceptor units, to planarize the molecular structure or, on the contrary, to increase the molecular twisting.

In the present work, a series of novel pyrazine quinoxaline derivatives with donor-acceptor (D-A) and donor- π -bridge-acceptor (D- π -A) structures are comprehensively investigated. The structures of the studied compounds are shown in Fig. 1. Compounds marked as **6a-c** and **7a-c** correspond to the D-A type of molecules, while the **8a-c** and **9a-c** extended molecules correspond to more complicated D- π -A type of systems. The thiophenyl moieties were incorporated into the compounds **8a-c** and **9a-c** to extend the overall length of conjugation. The influence of the electronic structure of azaheterocyclic fragment and conjugation effects on such important molecular properties like a light absorption and photoluminescence maxima were determined and discussed. The electroluminescence behavior of the synthesized compounds was checked for the fabricated non-doped light-emitting devices (OLEDs).

2. Experimental section

General Information. All reagents were purchased from commercial sources and were used without further purification. 2-Chloroquinoxaline (**2**) was obtained according to reported procedure [32]. 2-(5-Bromothiophen-2-yl)pyrazine (**3**), 2-(5-bromothiophen-2-yl)quinoxaline (**4**) and push-pull systems (**6a**, **7a**, **8a** and **9a**) were synthesized as described previously [33]. 1,4-Dioxane for the microwave-assisted Suzuki cross-coupling reaction were deoxygenated by bubbling argon for 1 h.

The ^1H and ^{13}C NMR spectra were recorded on a Bruker DRX-400, AVANCE-500 and AVANCE-600 instruments using Me_4Si as an internal standard. Elemental analysis was carried on a Eurovector EA 3000 automated analyzer. High resolution mass spectrometry was performed using a Bruker maXis Impact HD spectrometer. Melting points were determined on Boetius combined heating stages and were not corrected.

Flash-column chromatography was carried out using Alfa Aesar silica gel 0.040–0.063 mm (230–400 mesh), eluting with chloroform. The progress of reactions and the purity of compounds were checked by TLC on Sorbfil plates (Russia), in which the spots were visualized with UV light (λ 254 or 365 nm).

The XRD analysis of the single crystal of **6b** was carried out using an “Xcalibur 3” diffractometer on standard procedure (MoK-irradiation, graphite monochromator, ω -scans with 1° step, $T = 295(2)$ K). The empirical absorption correction was applied. Using Olex2, the structure was solved with the ShelXS structure solution program using Direct Methods and refined with the ShelXL refinement package using Least Squares minimization in anisotropic approximation for non-hydrogen atoms. The H-atoms were refined in isotropic approximation in the “rider” model. Deposition number CCDC 2022363 for **6b** contains the supplementary crystallographic data for this paper. These data can be obtained free of charge from the Cambridge Crystallographic Data Center via www.ccdc.cam.ac.uk/data_request/cif.

Microwave experiments were carried out in a Discover SP unimodal microwave system (CEM, USA) with a working frequency of 2.45 GHz and the power of microwave radiation ranged from 0 to 300 W. The reactions were carried out in a 35 mL reaction tube with the hermetic silicone cork. The temperature of the reaction was monitored using an inserted IR sensor by the external surface of the reaction vessel.

Absorption spectra of solutions of compounds were recorded ($1.0\text{--}3.0 \times 10^{-5}$ M) on a Solar CM2203 spectrophotometer. Fluorescence spectra of solutions and thermal vacuum deposition (TVD) films were recorded on a Varian Cary Eclipse fluorescence spectrophotometer. Delayed fluorescence and phosphorescence were measured with a delay of 200 μs after the excitation pulse for 5 ms. Low-temperature measurements were performed in an Optistat DN cryostat (Oxford Instruments). The absolute quantum yields of solutions and films obtained by thermal vacuum deposition were measured according to the literature procedure [34]. The quantum yields of pristine fluorescence at low temperatures were determined from the change in the area under the fluorescence spectrum at a fixed position of the samples in the cryostat.

Electrochemical studies of synthesized molecules were carried out using the Metrohm $\mu\text{Autolab}$ type III potentiostat. The standard three electrode cell equipped with platinum working electrode, Ag/AgNO_3 reference electrode and a glassy carbon rod counter electrode was employed. The cyclic voltammograms (CV) were registered in anhydrous CH_2Cl_2 with 5 mM of analyzed compound and 0.1 M tetrabutylammonium hexafluorophosphate as supporting electrolyte under N_2 atmosphere at a scan rate 100 mV/s. To HOMO-LUMO energies calculation, the potential of the reference electrode was calibrated by using the ferrocene/ferrocenium (Fc/Fc^+) redox couple $E_{1/2}(\text{Fc}/\text{Fc}^+)$ (that was estimated by the CV data as 0.54 V), which has a known oxidation

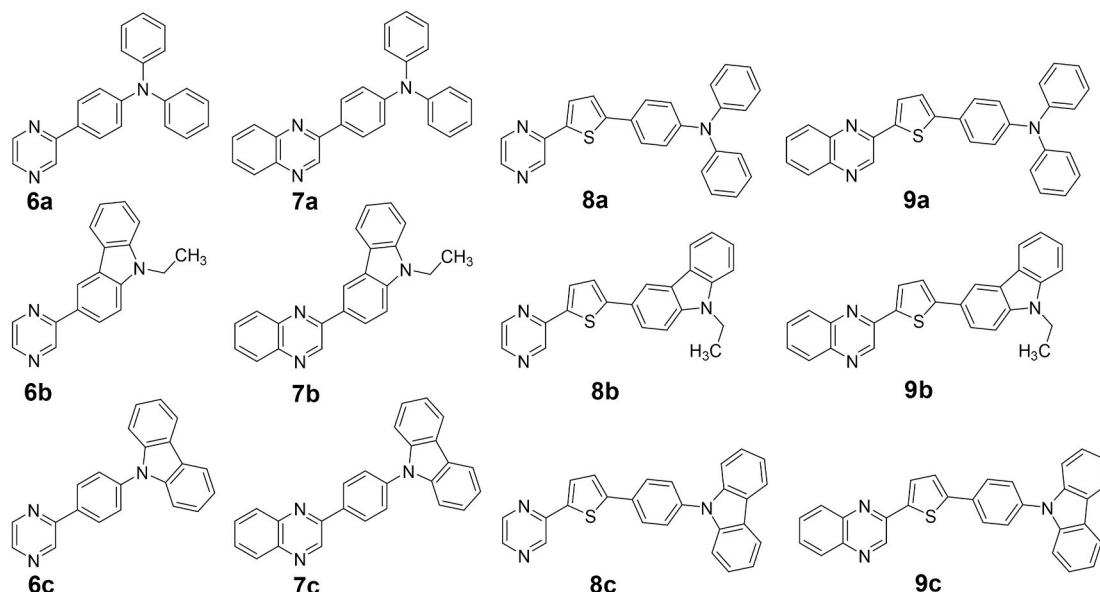


Fig. 1. The structures of pyrazine and quinoxaline-based D-A (**6a-c** and **7a-c**) and D- π -A (**8a-c** and **9a-c**) compounds studied in this work.

potential of +5.1 eV [35].

The HOMO and LUMO energy values were estimated from the onset potentials of the first independent oxidation and reduction process, respectively, according to the following equations:

$$E_{\text{HOMO}} (\text{eV}) = - [E_{\text{ox}}^{\text{onset}} - E_{1/2}(\text{Fc}/\text{Fc}^+) + 5.1]$$

$$E_{\text{LUMO}} (\text{eV}) = - [E_{\text{red}}^{\text{onset}} - E_{1/2}(\text{Fc}/\text{Fc}^+) + 5.1],$$

where $E_{1/2}(\text{Fc}/\text{Fc}^+)$ is the half-wave potential of the Fc/Fc^+ couple (in this work experimentally estimated as 0.54 V) against the Ag/Ag^+ electrode.

2.1. Molecular orbital calculation

Geometry optimizations of compounds 6–9 in the ground (S0) and first excited (S1) electronic states were performed by using the density functional theory (DFT) and its time-dependent version (TD-DFT) with the B3LYP [36] and PBE0 [37] hybrid functionals and 6-31G (d,p) basis set with the ORCA 4.0.3 program [38]. Visualization of molecular orbitals was made using the ChemCraft program [39].

2.2. Fabrication of OLED devices

The fabrication of non-doped OLEDs has been performed according to the literature procedure which has been described early [40]. OLED devices have the following structure: ITO (100 nm)/PEDOT:PSS (30 nm)/ α -NPD (22 nm)/emitting layer (EL) (35 nm)/BCP (15 nm)/LiF (1 nm)/Al (100 nm), where PEDOT:PSS is poly(2,3-dihydrothieno-1,4-dioxin)-poly(styrenesulfonate), α -NPD is *N,N'*-di(1-naphthyl)-*N,N'*-diphenyl-(1,1'-biphenyl)-4,4'-diamine, BCP is Bathocuproine, and EL is an emitting layer based on compounds 6–9. The layer thicknesses in OLED devices were determined by interferometry on a MicroXAM-100 optical profilometer (KLA Tencor) using reference samples placed in the deposition chamber together with working samples. The performance parameters, including current-voltage, current-brightness, and spectral characteristics were measured simultaneously by using a power supply Keithley 237 with an AvaSpec 2048 × 64 (Avantes) fiber-optic spectrometer with a collimation lens. The spectrometer in conjunction with an optical fiber and a collimation lens was preliminarily calibrated against an AvaSphere-50-LS-HAL-CAL lamp-sphere (Avantes) with a known spectral distribution in a solid angle to measure the absolute values of brightness.

General procedure for the Suzuki cross-coupling reactions for the synthesis of compounds 6–9: A mixture of the corresponding chloro-substituted (1 or 2) [or bromo-substituted (3 or 4)] 1,4-diazine (1.0 mmol), arylboronic derivative (5b or 5c) (1.2 mmol), $\text{Pd}(\text{PPh}_3)_4$ (58 mg, 5 mol %) and K_3PO_4 (530 mg, 2.5 mmol) was dissolved in 1,4-dioxane 15 mL. The reaction mixture was degassed and irradiated in a microwave apparatus at 160 °C (250 W) for 30 min. The reaction mixture was cooled, filtered, and dissolved in a mixture of EtOAc and water (1:1, 50 mL), and the organic layer was separated. The aqueous layer was extracted with EtOAc (2 × 25 mL). The combined organic extracts were dried with MgSO_4 and the solvents evaporated. Purification by silica gel column chromatography with EtOAc/hexane (1:4, v/v) as an eluent to afford the desired cross-coupling products.

9-Ethyl-3-(pyrazin-2-yl)-9H-carbazole (6b). Yield 202 mg (74%), grey solid, mp 103–105 °C. ^1H NMR (500 MHz, CDCl_3) δ 9.19 (d, $J = 1.5$ Hz, 1H), 8.83 (d, $J = 1.7$ Hz, 1H), 8.67 (dd, $J = 2.5, 1.6$ Hz, 1H), 8.49 (d, $J = 2.5$ Hz, 1H), 8.23 (dt, $J = 7.7, 0.9$ Hz, 1H), 8.18 (dd, $J = 8.6, 1.8$ Hz, 1H), 7.57–7.51 (m, 2H), 7.47 (d, $J = 8.2$ Hz, 1H), 7.35–7.30 (m, 1H), 4.43 (q, $J = 7.2$ Hz, 2H), 1.50 (t, $J = 7.3$ Hz, 3H). ^{13}C NMR (126 MHz, CDCl_3) δ 153.7, 144.0, 142.0, 141.7, 141.0, 140.5, 127.1, 126.2, 124.5, 123.6, 123.0, 120.7, 119.4, 119.3, 108.9, 108.8, 37.7, 13.8. HRMS (ESI): m/z calcd for $\text{C}_{18}\text{H}_{16}\text{N}_3$: 274.1339 [M+H] $^+$; found: 274.1335.

9-Ethyl-3-(quinoxalin-2-yl)-9H-carbazole (7b). Yield 239 mg (74%), pale yellow solid, mp 191–192 °C. ^1H NMR (500 MHz, CDCl_3) δ

9.49 (s, 1H), 8.98 (d, $J = 1.7$ Hz, 1H), 8.36 (dd, $J = 8.6, 1.8$ Hz, 1H), 8.25 (dd, $J = 7.8, 1.0$ Hz, 1H), 8.19 (dd, $J = 8.4, 1.4$ Hz, 1H), 8.12 (dd, $J = 8.3, 1.4$ Hz, 1H), 7.79 (ddd, $J = 8.4, 6.9, 1.5$ Hz, 1H), 7.72 (ddd, $J = 8.3, 6.8, 1.4$ Hz, 1H), 7.58 (d, $J = 8.6$ Hz, 1H), 7.53 (ddd, $J = 8.2, 7.0, 1.1$ Hz, 1H), 7.47 (d, $J = 8.1$ Hz, 1H), 7.35–7.28 (m, 1H), 4.44 (q, $J = 7.3$ Hz, 2H), 1.50 (t, $J = 7.3$ Hz, 3H). ^{13}C NMR (126 MHz, CDCl_3) δ 152.6, 143.6, 142.5, 141.2, 141.1, 140.5, 130.1, 129.3, 129.1, 128.8, 127.6, 126.2, 125.2, 123.7, 123.1, 120.8, 120.0, 119.5, 109.0, 108.8, 37.8, 13.8. HRMS (ESI): m/z calcd for $\text{C}_{18}\text{H}_{18}\text{N}_3$: 324.1495 [M+H] $^+$; found: 324.1497. Data similar to the literature [41].

9-Ethyl-3-[5-(pyrazin-2-yl)thiophen-2-yl]-9H-carbazole (8b). Yield 231 mg (65%), yellow solid, mp 171–172 °C. ^1H NMR (500 MHz, CDCl_3) δ 8.97 (d, $J = 1.6$ Hz, 1H), 8.51 (dd, $J = 2.6, 1.6$ Hz, 1H), 8.38 (dd, $J = 10.9, 2.2$ Hz, 2H), 8.15–8.10 (m, 1H), 7.78 (dd, $J = 8.5, 1.8$ Hz, 1H), 7.68 (d, $J = 3.8$ Hz, 1H), 7.50 (ddd, $J = 8.2, 7.0, 1.2$ Hz, 1H), 7.43–7.38 (m, 3H), 7.29–7.25 (m, 1H), 4.37 (q, $J = 7.2$ Hz, 2H), 1.45 (t, $J = 7.2$ Hz, 3H). ^{13}C NMR (126 MHz, CDCl_3) δ 149.5, 148.7, 144.0, 141.8, 140.4, 140.3, 139.9, 138.8, 126.9, 126.1, 124.9, 124.0, 123.4, 123.1, 122.8, 120.6, 119.7, 117.9, 108.9, 108.7, 37.7, 13.8. HRMS (ESI): m/z calcd for $\text{C}_{22}\text{H}_{18}\text{N}_3\text{S}$: 356.1216 [M+H] $^+$; found: 356.1214.

9-Ethyl-3-[5-(quinoxalin-2-yl)thiophen-2-yl]-9H-carbazole (9b). Yield 247 mg (61%), yellow solid, mp 171–172 °C. ^1H NMR (500 MHz, CDCl_3) δ 9.22 (s, 1H), 8.42 (d, $J = 1.7$ Hz, 1H), 8.13 (d, $J = 7.7$ Hz, 1H), 8.05 (ddd, $J = 11.7, 8.3, 1.4$ Hz, 2H), 7.85–7.79 (m, 2H), 7.73 (ddd, $J = 8.4, 6.9, 1.5$ Hz, 1H), 7.66 (ddd, $J = 8.2, 6.9, 1.4$ Hz, 1H), 7.49 (ddd, $J = 8.2, 7.0, 1.1$ Hz, 1H), 7.45–7.37 (m, 3H), 7.30–7.22 (m, 1H), 4.35 (q, $J = 7.3$ Hz, 2H), 1.44 (t, $J = 7.2$ Hz, 3H). ^{13}C NMR (126 MHz, CDCl_3) δ 150.4, 147.5, 142.2, 141.9, 141.1, 140.4, 139.9, 139.7, 130.3, 129.1, 128.9, 128.8, 128.2, 126.1, 124.9, 124.0, 123.4, 123.1, 122.8, 120.6, 119.3, 118.0, 108.8, 108.7, 37.7, 13.8. HRMS (ESI): m/z calcd for $\text{C}_{26}\text{H}_{20}\text{N}_3\text{S}$: 406.1372 [M+H] $^+$; found: 406.1371.

9-[4-(Pyrazin-2-yl)phenyl]-9H-carbazole (6c). Yield 257 mg (80%), off-white solid, mp 149–150 °C (ref. [33] 146–147 °C). ^1H NMR (400 MHz, CDCl_3) δ 9.15 (d, $J = 1.6$ Hz, 1H), 8.70 (dd, $J = 2.5, 1.6$ Hz, 1H), 8.58 (d, $J = 2.5$ Hz, 1H), 8.31–8.24 (m, 2H), 8.16 (dt, $J = 7.7, 1.0$ Hz, 2H), 7.80–7.72 (m, 2H), 7.50 (dt, $J = 8.3, 1.0$ Hz, 2H), 7.44 (ddd, $J = 8.2, 6.9, 1.2$ Hz, 2H), 7.32 (ddd, $J = 8.0, 7.0, 1.2$ Hz, 2H). ^{13}C NMR (126 MHz, CDCl_3) δ 151.9, 144.3, 143.2, 142.1, 140.5, 139.3, 135.1, 128.4, 127.4, 126.1, 123.6, 120.4, 120.3, 109.8. HRMS (ESI): m/z calcd for $\text{C}_{22}\text{H}_{16}\text{N}_3$: 322.1339 [M+H] $^+$; found: 322.1339. Data similar to the literature [42].

9-[4-(Quinoxalin-2-yl)phenyl]-9H-carbazole (7c). Yield 290 mg (78%), pale yellow solid, mp 196–198 °C. ^1H NMR (400 MHz, CDCl_3) δ 9.44 (s, 1H), 8.49–8.43 (m, 2H), 8.24–8.14 (m, 4H), 7.87–7.77 (m, 4H), 7.53 (dt, $J = 8.3, 0.9$ Hz, 2H), 7.45 (ddd, $J = 8.3, 7.0, 1.3$ Hz, 2H), 7.33 (ddd, $J = 8.1, 7.1, 1.1$ Hz, 2H). ^{13}C NMR (126 MHz, CDCl_3) δ 150.9, 143.1, 142.3, 141.7, 140.5, 139.6, 135.6, 130.5, 129.8, 129.6, 129.2, 129.1, 127.4, 126.1, 123.7, 120.4, 120.3, 109.8. HRMS (ESI): m/z calcd for $\text{C}_{26}\text{H}_{18}\text{N}_3$: 372.1495 [M+H] $^+$; found: 372.1488.

9-[4-[5-(Pyrazin-2-yl)thiophen-2-yl]phenyl]-9H-carbazole (8c). Yield 265 mg (65%), pale yellow solid, mp 202–203 °C. ^1H NMR (500 MHz, CDCl_3) δ 8.99 (d, $J = 1.5$ Hz, 1H), 8.53 (dd, $J = 2.6, 1.6$ Hz, 1H), 8.42 (s, 1H), 8.15 (dt, $J = 7.8, 0.9$ Hz, 2H), 7.91–7.87 (m, 2H), 7.70 (d, $J = 3.9$ Hz, 1H), 7.64–7.61 (m, 2H), 7.48–7.40 (m, 5H), 7.30 (ddd, $J = 7.9, 6.9, 1.2$ Hz, 2H). ^{13}C NMR (126 MHz, CDCl_3) δ 148.3, 146.7, 144.0, 142.4, 140.8, 140.6, 140.4, 137.5, 132.8, 127.5, 127.2, 126.9, 126.0, 124.7, 123.5, 120.3, 120.1, 109.8. HRMS (ESI): m/z calcd for $\text{C}_{26}\text{H}_{18}\text{N}_3\text{S}$: 404.1216 [M+H] $^+$; found: 404.1217.

9-[4-[5-(Quinoxalin-2-yl)thiophen-2-yl]phenyl]-9H-carbazole (9c). Yield 259 mg (57%), pale yellow solid, mp 216–217 °C. ^1H NMR (600 MHz, CDCl_3) δ 9.31 (s, 1H), 8.19 (dt, $J = 7.8, 1.0$ Hz, 2H), 8.12 (td, $J = 8.4, 1.3$ Hz, 2H), 8.00–7.95 (m, 2H), 7.92 (d, $J = 3.9$ Hz, 1H), 7.80 (ddd, $J = 8.4, 6.8, 1.5$ Hz, 1H), 7.75 (ddd, $J = 8.3, 6.9, 1.5$ Hz, 1H), 7.71–7.65 (m, 2H), 7.56–7.49 (m, 3H), 7.47 (ddd, $J = 8.2, 7.0, 1.2$ Hz, 2H), 7.34 (ddd, $J = 7.9, 6.9, 1.0$ Hz, 2H). ^{13}C NMR (151 MHz, CDCl_3) δ 147.5, 147.2, 142.2, 141.8, 141.8, 141.4, 140.6, 137.7, 132.8, 130.6,

129.3, 129.2, 129.1, 128.1, 127.5, 127.3, 126.1, 124.8, 123.6, 120.4, 120.2, 109.8. HRMS (ESI): m/z calcd for $C_{30}H_{20}N_3S$: 454.1372 $[M+H]^+$; found: 454.1373.

3. Results and discussion

3.1. Synthesis

We recently synthesized triphenylamine substituted derivatives (**6a**, **7a**, **8a**, and **9a**) that can be used as effective fluorescence chemosensors for the detection of nitroaromatic compounds and amines [33]. Another linear push-pull systems **6–9** were similarly obtained in good yields by microwave-assisted Suzuki cross-coupling reaction from readily available 2-chloro- and 2-(5-bromothiophen-2-yl)-substituted pyrazines (**1,3**) and quinoxalines (**2,4**) (Scheme 1) [32,33]. The structural evidence was accrued by 1H and ^{13}C NMR, HRMS, and corresponded well with their expected structures. The structure of **6b** was established unequivocally by X-ray diffraction analysis (Fig. 2).

3.2. The UV-vis and photoluminescence (PL) spectroscopic data

The optical properties of the prepared D-(π)-A type 1,4-diazine-based dyes **6–9** have been studied by UV/vis and photoluminescence (PL) spectroscopy both in solution ($CHCl_3$ and EtOH) and solid state (TVD films) at different temperatures. The results of these studies are summarized in Table 1 (Supplementary Material, Figs. S17–S60). Recently, it has been shown that triphenylamine-substituted compounds **6a**, **7a**, **8a**, and **9a** exhibit effective luminescence in non-polar and low-polar solvents [33]. Here we have demonstrated that the relative quantum fluorescence yields of compounds **6–9** in a chloroform solution are 50–95% (Table 1). On the other hand, in polar solvents such as

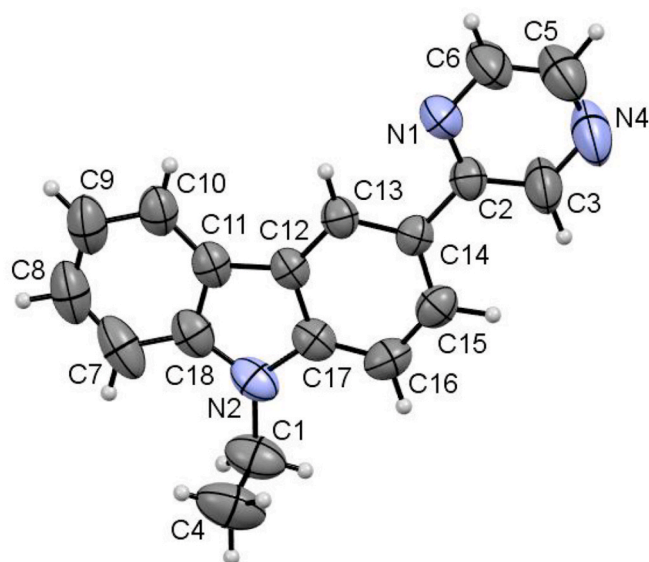
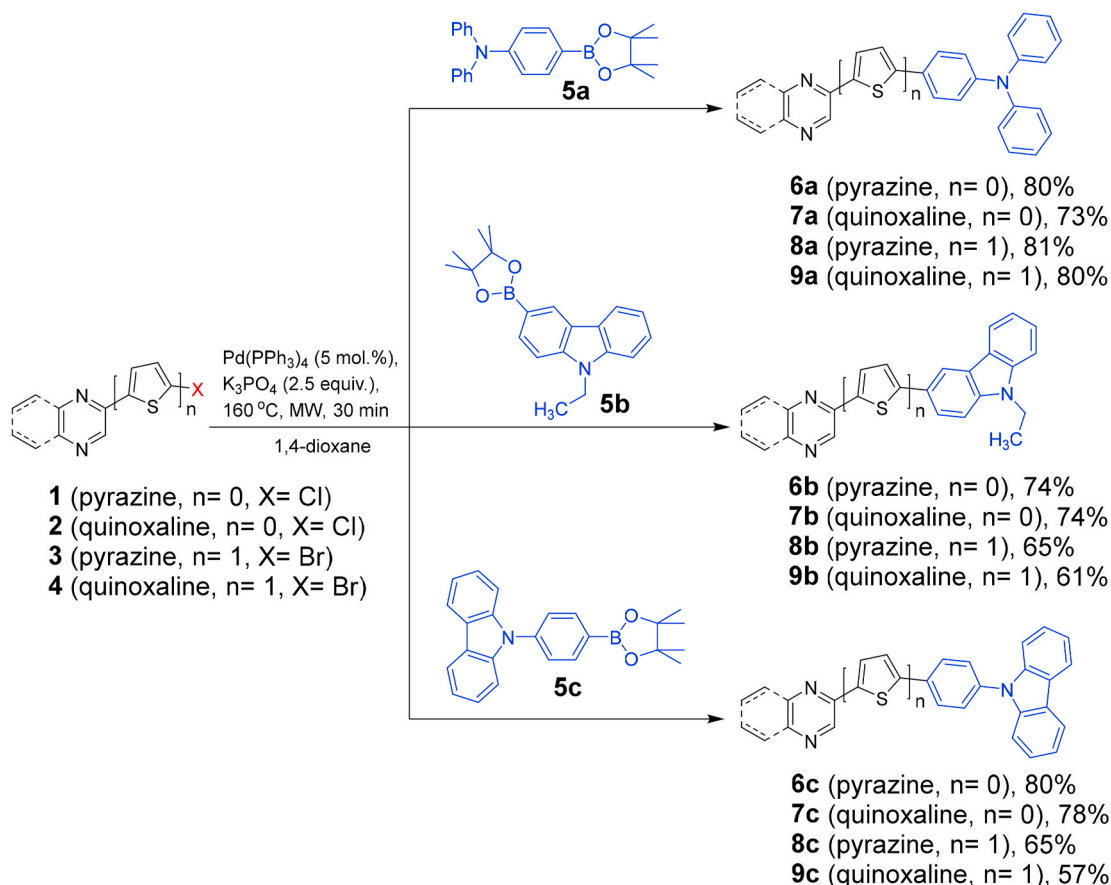


Fig. 2. ORTEP of **6b** with thermal ellipsoids are at 50% probability level.

ethanol, the fluorescence efficiency at room temperature ϕ_f^{293} dramatically decreases below 10%. It has been shown that for push-pull systems based on quinoxaline **9a–c** in ethanol solutions, decreasing the temperature from 293 to 77 K leads to a significant increase in the fluorescence intensity ϕ_f^{77} (see Figs. S27, S31, S35).

Moreover, this is accompanied by significant shifts of the maxima of both emission bands and fluorescence excitation (see Table 1 and Figs. S28, S32, S36), which indicates the charge-transfer nature of these



Scheme 1. Synthetic route to the linear push-pull systems **6–9**.

Table 1

Absorption maxima λ_{abs} and extinction coefficient (ϵ) in chloroform, fluorescence (λ_{fl}) and fluorescence excitation maxima (λ_{ex}), PLQY (ϕ_{fl}) and phosphorescence maxima (λ_{phos}) in ethanol at 293 and 77 K.

Compound	Chloroform		Ethanol			
	λ_{abs} , nm (ϵ , $l \times \text{mol}^{-1} \times \text{cm}^{-1}$)	λ_{fl} , nm (ϕ)	$\lambda_{\text{ex}}^{293}$, nm (λ_{ex}^{77} , nm)	$\lambda_{\text{fl}}^{293}$, nm (λ_{fl}^{77} , nm)	ϕ_{fl}^{293} , (ϕ_{fl}^{77})	$\lambda_{\text{phos}}^{77}$, nm (τ_{phos}^{77} , ms)
6a	370 (19900)	494 (0.51)	368	530	0.008	–
6b	338 (14500)	422 (0.94)	338	487	0.026	–
6c	340 (13700)	450 (0.95)	338	490	0.001	–
7a	408 (24900)	553 (0.61)	408 (450)	600 (493)	0.002 (0.2)	590 (355)
7b	384 (18000)	478 (0.66)	388	540	0.02	–
7c	366 (13000)	498 (0.68)	364	560	0.006	–
8a	404 (10600)	518 (0.83)	398	554	0.03	–
8b	388 (8500)	488 (0.86)	386	540	0.009	–
8c	368 (19300)	464 (0.89)	366	510	0.12	–
9a	433 (31600)	582 (0.56)	433 (482)	626 (524)	0.002 (0.07)	670 (3)
9b	420 (28600)	540 (0.58)	420 (461)	600 (506)	0.03 (0.98)	648 (10.6)
9c	398 (20900)	508 (0.75)	400 (436)	545 (477)	0.008 (0.08)	686 (5.7)

transitions. The strong temperature dependence of the position of maxima in the absorption, excitation and fluorescence spectra for compounds in polar solvents could be the convincing evidence of their charge-transfer nature [43,44].

On cooling solutions **9a-c**, the fluorescence maximum undergoes a hypsochromic shift with a simultaneous decrease in the bandwidth, while the longwave excitation maximum, on the contrary, has a bathochromic shift and increases in intensity. For example, for **9b** in an ethanol solution, the absorption maximum shifts from 433 nm to 482 nm (Fig. 3a and S32), the fluorescence maximum shifts from 600 nm to 506 nm (Fig. 3b and S31), and the fluorescence quantum yield increases from 3% to 98% with decreasing temperature (Table 1).

Slightly different results have been achieved in amorphous films obtained by thermal vacuum deposition (Table 2, Figs. S37–S66). Due to the limited rotation of molecular fragments relative to each other, they do not have significant geometric changes upon transition to an excited state even when cooled to 77 K. This leads to the fact that the quantum yields ϕ_{fl} of amorphous TVD films changes little over a wide temperature range (Table 2). The lowest values of the fluorescence quantum yield

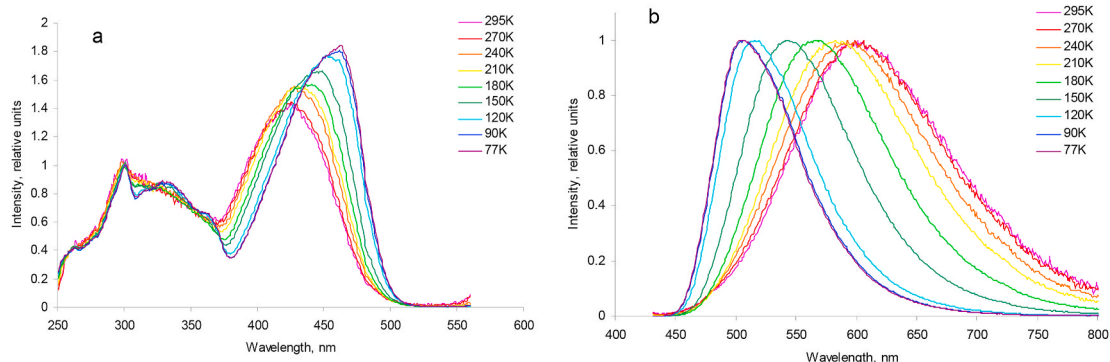


Fig. 3. Normalized excitation (a) and fluorescence spectra (b) of **9b** in ethanol at different temperatures.

Table 2

Prompt fluorescence maxima λ_{fl} , PLQY at 293 and 77 K (ϕ_{fl}), DF maxima λ_{df} , DF lifetime at 293 K and 77 K (τ_{df}), type of DF, maxima of phosphorescence (λ_{phos}), and lifetime of phosphorescence at 293 and 77 K (τ_{phos}) of D-(π)-A push-pull systems in TVD films.

Compound	λ_{fl} , nm	ϕ_{fl}^{293} , (ϕ_{fl}^{77})	λ_{df} , nm	τ_{df}^{293} , ms (τ_{df}^{77} , ms) ^a	DF type	λ_{phos} , nm	τ_{phos}^{293} , ms (τ_{phos}^{77} , ms) ^a
6a	490	0.03 (0.03)	460	–	–	590	2.2 (29.7)
6b	433	0.03 (0.02)	–	–	–	580	5.0 (135)
6c	418	0.01 (0.01)	–	–	–	550	3.7 (70)
7a	475	0.07 (0.20)	472	3.8 (10)	TTA + HE	688	2.5 (23.2)
7b	482	0.05 (0.22)	490	3.6 (3.8)	TTA	658	5 (13.6)
7c	465	0.02 (0.05)	465	–	–	590	– (22.3)
8a	525	0.04 (0.06)	560	–	–	733	– (6.8)
8b	477	0.02 (0.03)	477	– (3.6)	–	706	1.5 (4.7)
8c	545	0.01 (0.01)	550	–	–	690	– (5)
9a	555	0.10 (0.24)	565	5.4 (7)	TTA	690	– (3.5)
9b	567	0.06 (0.10)	570	– (6)	TTA	705	– (6.7)
9c	529	0.11 (0.15)	529	2.4 (6.5)	HE	740	1.1 (3.2)

^a The kinetics of delayed fluorescence can be described by three-exponential decay, and the kinetics of phosphorescence by mono-two-exponential decay (see Tables S1–S5 in Supplementary Material). Table 2 shows only the longest of lifetimes.

(0.01–0.04) are characteristic of compounds containing the pyrazine ring as an acceptor fragment (**6a-c** and **8a-c**). In general, the fluorescence efficiency of compounds containing quinoxaline (**7a-c** and **9a-c**) in TVD films is higher (0.02–0.11). It should be noted that with decreasing temperature, a more significant increase in the fluorescence efficiency ϕ_{fl}^{77} was observed up to values of 0.1–0.24, and the emission maxima shifted to longer wavelengths, in comparison with pyrazine analogs (see λ_{fl} in Table 2).

Besides, the presence of quinoxaline in the structure of push-pull system leads to the appearance of delayed fluorescence (DF). It is known, that the nature of DF can be different: either it is thermally activated delayed fluorescence (TADF) [45], which is effectively implemented at sufficiently high temperatures (for example, room temperature) and a small energy gap between S1 and T1 (or higher T2, T3, etc.) [46]. This type of thermal activation of the fluorescence in the literature is often referred to as “hot-exciton” (HE) states, or triplet-triplet annihilation (TTA) [47], which is not so critical to

temperature in the case of densely packed molecules in TVD films. A characteristic feature of TADF and HE is that the process efficiency drops sharply with decreasing temperature, while in molecules **7a** and **7b**, the DF intensity increases with decreasing temperature to 77 K. This is most likely due to triplet-triplet annihilation (TTA) rather than TADF or HE (Fig. S44, S48).

In particular, delayed fluorescence for **7b** in a wide temperature range occurs at almost the same time (Table S2, Fig. S49). According to literature data [48], a mixed type of radiation (TTA + TADF, or in this case, TTA + HE) is possible for **7a** at high temperature because the contrary of **7b**, for this compound, the DF lifetime increases non-monotonically with increasing temperature (Fig. S45, Table S1).

Notably, intense delayed fluorescence for compound **9c** is observed at temperatures near room temperature through the thermal activation mechanism of “hot-exciton” (HE) with a maximum intensity at 529 nm, which strongly decreases at low temperature (Fig. 4b and S64). In this case, the duration of radiation increases by 2.7 times (Fig. S65), and the radiation is characterized by multi-exponential decay (Table S5).

To rationalize obtained results, quantum chemical calculations of the energies of the S_1 , T_1 , and T_2 states for the ground and excited states geometry have been made (Tables S6-S-17, Fig. 5 and S67-S78). By the fact that phosphorescence at 740 nm (Fig. 4b, S64 and S65, Table S5) is observed at 77 K, it can be assumed that the second triplet state T_2 , which is energy-degenerate with S_1 , plays a significant role for compound **9c** [49]. Due to the rather large energy band gap between T_1 and T_2 , approximately 5400 cm^{-1} (calculated from the difference between the S_1 and T_1 states). Besides, due to the presumably different orbital nature, no internal conversion occurs between these states, because of which the T_2 state has a lifetime sufficient for the realization of inverse intersystem crossing to the S_1 state. To evidence, quantum chemical calculations have been performed for compound **9c** (Table S17, Fig. 5

and S78).

It was found that in the geometry of the excited S_1 state, the acceptor fragment and the π -linker of the push-pull system are flattened in comparison with the geometry of the ground state. At the same time, the torsion angle between the carbazole and phenyl fragments increases from 52.9° to 80.4° . This significantly enhances the charge-transfer nature of the S_1 and T_2 transitions and leads to a small overlap integral of molecular orbitals responsible for the transition [50]. At the same time, the T_1 transition becomes locally excited on the acceptor – π -linker fragment. This energy diagram (Fig. S78) explains the strong temperature dependence of the delayed fluorescence intensity and is typical for compounds emitting by the “hot-exciton” mechanism [49].

It worth noting that “hot-exciton” usually means the initial excitation product caused by photogeneration or charge recombination, for example, it is considered as an exciton with kinetic energy E_K that considerably exceeds the mean thermal energy $k_B T_L$, i.e., $E_K > k_B T_L$, where k_B is the Boltzmann constant, and T_L refers to the lattice temperature of the solid [51].

An interesting feature of TVD film **9c** is its transition to a more ordered structure after freezing to 77 K and exposure to light at 400 nm, which manifests itself in the appearance of a vibronic structure of the emission band of both prompt and delayed fluorescence (comparison Figs. 4a and 4c vs. Figs. 4b and 4d).

It was shown that the introduction of thiophene linker (compounds **8a-c** and **9a-c**) into the conjugation chain leads to a long-wavelength shift of the absorption and emission bands, which is associated with an increase in the length of the conjugation chain, as well as a significant reduction in the observed phosphorescence lifetime τ_{phos}^{77} (from tens and hundreds of milliseconds to units of milliseconds), both in TVD films (Table 2) and in solutions (Table 1), which is especially clearly observed at low temperatures. For example, for compound **6b** in a TVD film, the

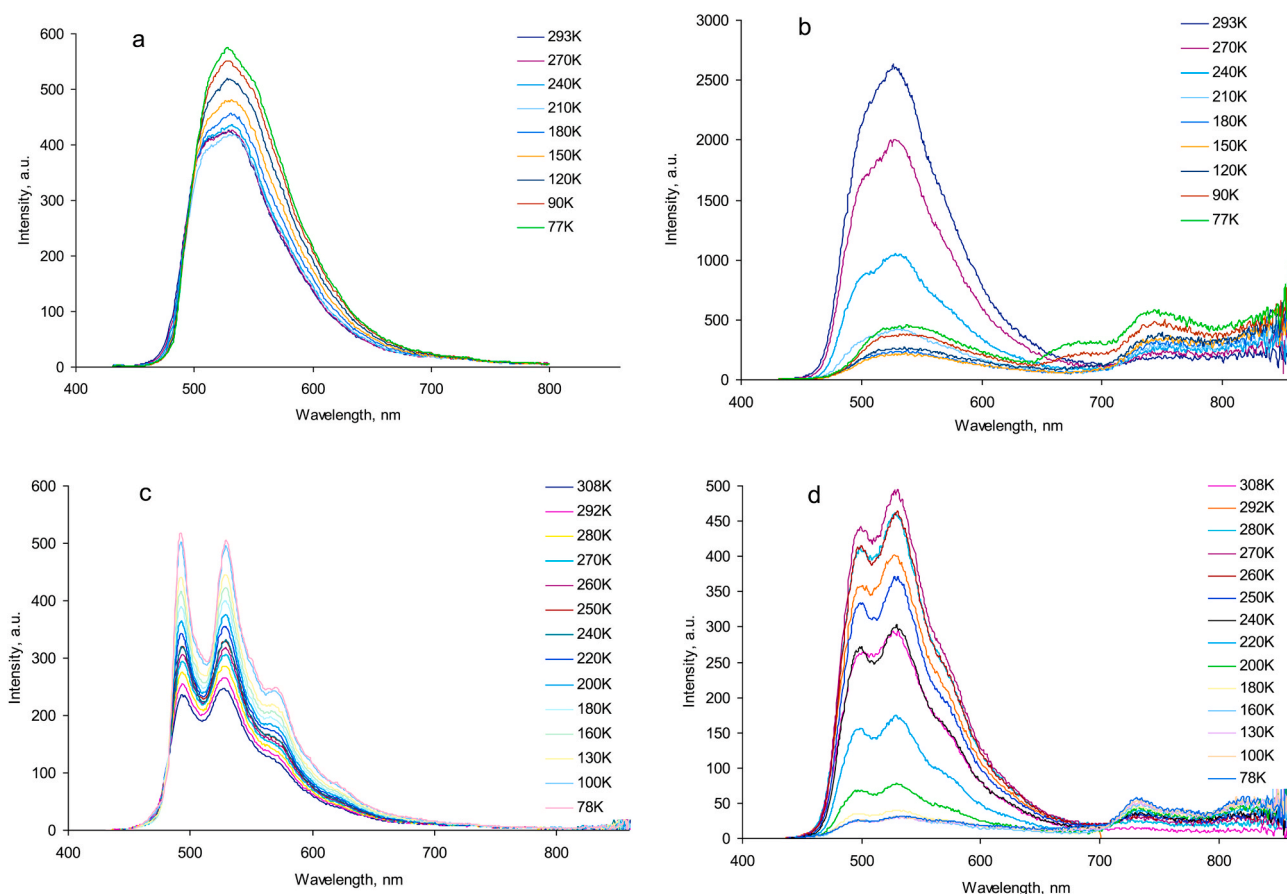


Fig. 4. Prompt (a,c) and delayed (b,d) fluorescence spectra for TVD film **9c** before (a,b) and after (c,d) the transfer into a vibronic structure.

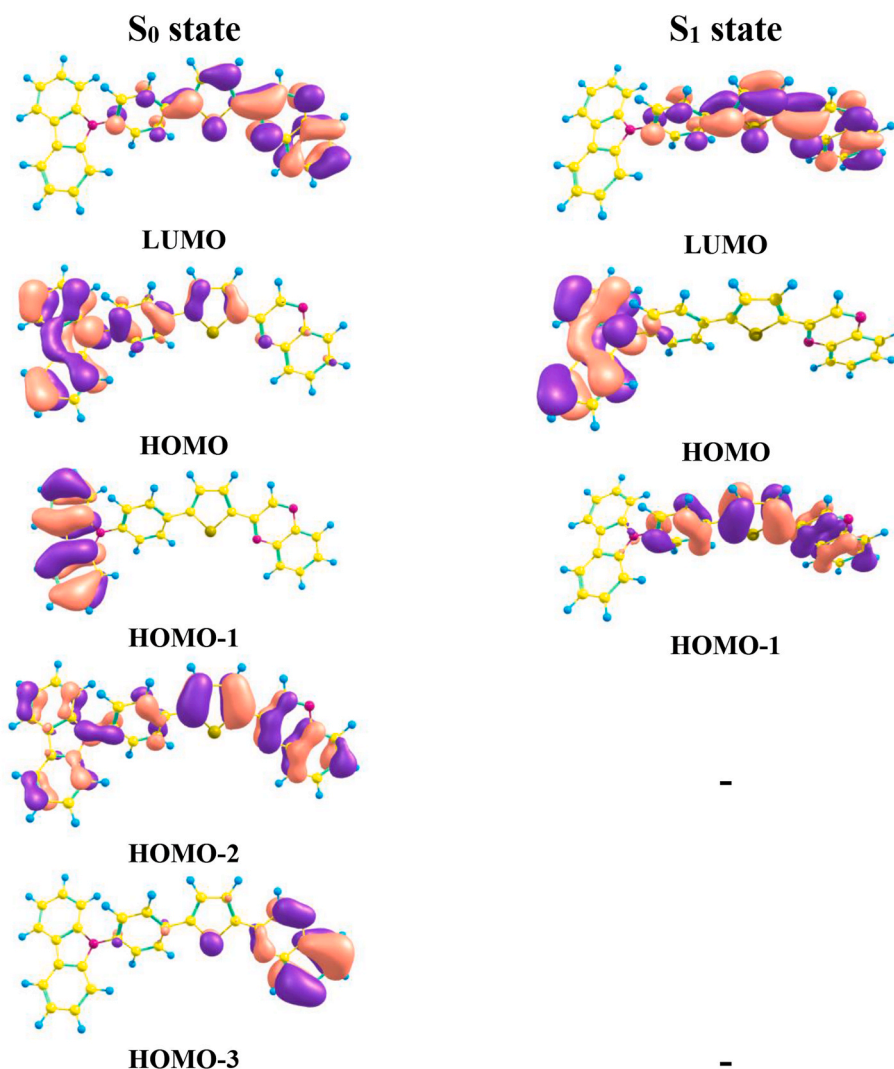


Fig. 5. Contour plots (isovalue = 0.03) of the frontier orbitals of **9c** at the optimized ground (S_0) and first singlet excited state (S_1) geometry.

observed phosphorescence lifetime $\tau_{\text{phos}}^{\text{77}}$ is 135 ms, while for its thiophene-containing analog **8b** this time is only 4.7 ms.

3.3. Electrochemistry

Cyclic voltammetry (CV) was applied to study the electrochemical character of synthesized compounds and to determine their redox potentials. The cyclic voltammograms shown in Figs. S79–S86

Table 3
Estimated HOMO-LUMO energies of the fluorophores **6–9**.

Compound	$E_{\text{Ox}}^{\text{onset}}$, V (vs Ag/Ag ⁺)	$E_{\text{Red}}^{\text{onset}}$, V (vs Ag/Ag ⁺)	E_{HOMO} , eV	$E_{\text{LUMO}}^{\text{opt}}$, eV	$\epsilon_{\text{ELUMO}}^{\text{el}}$, eV	λ_{onset}	$E_{\text{g}}^{\text{opt}}$, eV	$\epsilon_{\text{g}}^{\text{el}}$, eV
6a ^a	1.34	–	–5.94	–2.97	–	–	2.97 ^d	–
7a ^a	0.97	–	–5.42	–2.77	–	–	2.65 ^d	–
8a ^a	0.86	–	–5.42	–2.75	–	–	2.67 ^d	–
9a ^a	0.84	–	–5.40	–2.91	–	–	2.49 ^d	–
6b	1.40	–1.45	–5.96	–3.26	–3.11	459	2.70	2.85
7b	1.20	–1.55	–5.76	–3.17	–3.01	481	2.58	2.75
8b	0.75	–	–5.31	–2.80	–	494	2.51	–
9b	1.10	–1.40	–5.66	–3.23	–3.16	510	2.43	2.5
6c	1.35	–	–5.91	–3.03	–	431	2.88	–
7c	1.24	–1.60	–5.80	–3.07	–2.96	454	2.73	2.84
8c	1.15	–	–5.71	–3.10	–	475	2.61	–
9c	1.17	–1.32	–5.73	–3.30	–3.24	510	2.43	2.49

^a The early obtained data [33].

^b $E_{\text{LUMO}}^{\text{opt}} = E_{\text{gap}} - E_{\text{HOMO}}$.

^c Estimated from the $E_{\text{Red}}^{\text{onset}}$.

^d Energy gap estimated from the onset of the absorption spectra recorded in CH₂Cl₂ solution ($E_{\text{g}}^{\text{opt}} = 1240/\lambda_{\text{onset}}$).

^e Energy gap estimated from the electrochemical data.

demonstrate two pronounced oxidation peaks in the potential range 1.5–2 V and for some of them are quasi-reversible reduction process in -1 - (-2) V. There are not any cathodic peaks for **8b** and **8c** have been observed on the CV. On the base of the electrochemical and optical experimental data (see S79–S86 and S87), the HOMO and LUMO energy values were estimated (see Table 3). It can be seen that the electrochemical band gaps a little wider than the optical one. HOMO energies of compounds containing a carbazolyl group are between -5.96 eV and -5.6 eV, i.e. in general lower than for compounds with triphenylamine group (-5.4 eV), while LUMO is between -2.75 eV and -3.30 eV. These results have been used to optimize the charge-transport layers of the fabricated OLEDs.

3.4. Electroluminescence properties

To explore their applicable potential application in OLEDs, vacuum-deposited nondoped devices were fabricated based with the optimized configuration of ITO (100 nm)/PEDOT:PSS (30 nm)/ α -NPD (22 nm)/EL (35 nm)/BCP (15 nm)/LiF (1 nm)/Al (100 nm), where ITO (indium tin oxides) and Al were used as the anode and cathode respectively, α -NPD served as the hole transporting layer, BCP (Bathocuproine) served as the electron transporting and hole block layer and LiF served as the electron injection layer (for example, see Fig. 6).

The key performance parameters of the devices are summarized in Table 4 and Fig. 7 and S88–S135.

Compounds bearing triphenylamine as a donor layer have shown higher efficiency of OLED devices, especially when the BCP layer is added. This behavior is due to the fact that the HOMO levels of compounds **7a**, **8a**, and **9a** (-5.42 , -5.42 , and -5.4 eV, respectively, in Table 3) are in good agreement with the HOMO level of the hole-transport layer of α -NPD (-5.4 eV) [52], and the addition of a BCP layer creates a barrier for holes that do not interact with electrons, since the HOMO level for BCP is -6.5 eV [53]. The HOMOs of carbazole-containing compounds **6b–9b** and **6c–9c**, as well as **6a**, are lower in energy in the range from -5.3 to -5.96 eV (Table 3); therefore, a sufficiently large potential barrier appears between α -NPD and these compounds.

The devices demonstrate the characteristic change in the color of electroluminescence from blue (for compounds **6a–c**) to green (for **7a–c** and **8a–c**) and yellow (for **9a–c**). Probably, it can be explained by an increase in the length of the conjugated push-pull system and by loss of

Table 4

Electroluminescent properties [emission maxima λ_{el} , turn-on voltage U_{on} , maximal brightness B_{max} at voltage (V), current efficiency $\phi(1000)$ and external quantum efficiency EQE(1000) (at brightness of 1000 cd/m²)] of non-doped devices **6–9** with the structure of ITO (100 nm)/PEDOT:PSS (30 nm)/ α -NPD (22 nm)/EL (35 nm)/BCP (15 nm)/LiF (1 nm)/Al (100 nm).

Compound	λ_{el} , nm	U_{on} , V	B_{max} , cd/m ² (V)	$\phi(1000)$, cd/A	EQE(1000), %
6a	450	8.5	41 (12)	0.04 ^a	–
6b	447	6.4	81 (14)	0.03 ^a	–
6c	454	8.8	180 (15)	0.12 ^a	–
7a	510	3.8	6770 (10)	2.03	0.61
7b	491	4.9	2017 (12)	0.67	0.27
7c	452/ 600	11.2	10 (15)	0.01 ^a	–
8a	495	5.5	2970 (12)	0.65	0.23
8b	477	6.5	2084 (15)	0.27	0.12
8c	522	7.5	190 (15)	0.02 ^a	–
9a	555	3.2	31565 (10)	4.27	1.26
9b	567	3.9	3500 (10)	1.38	0.53
9c	545	4.8	1554 (16)	0.98	0.34

^a Current efficiency given at maximum achieved brightness.

energy because of non-radiative transitions. The maximum of electroluminescence for most compounds lies in the same region as prompt fluorescence, except for compound **7c**. Fluorophore **7c** has two maxima of electroluminescence with very low intensity at 450 and 600 nm (Fig. S110), which is most likely associated with the simultaneous emission of the α -NPD layer [54] and the exciplex at the α -NPD/**7c** interface due to the large potential barrier between the HOMO levels of these compounds.

Despite the low values of the fluorescence quantum yield of TVD films of the compound (**7a,b** and **9a–c**), which had a delayed fluorescence, OLEDs based on them demonstrated sufficiently high brightness and efficiency (Fig. S100–S107, S124–S135). Apparently, this can be explained with the formation of “hot excitons” [49]. In addition, there is no potential barrier at the α -NPD/**9a** interface for the **9a**-based device (Fig. S124). Fig. 7 shows the current-voltage and current-brightness characteristics of an OLED based on compound **9a**, which showed the best current efficiency of 4.2 cd/A and brightness of 31565 cd/m².

The external quantum efficiency EQE is related to the internal efficiency of the IQE by the equation $EQE = IQE \times \eta_{out} = \beta_{ST} \times \phi_{fl} \times \eta_{out} \times \gamma_{eh}$ [49], where η_{out} is the coefficient of light output from the OLED

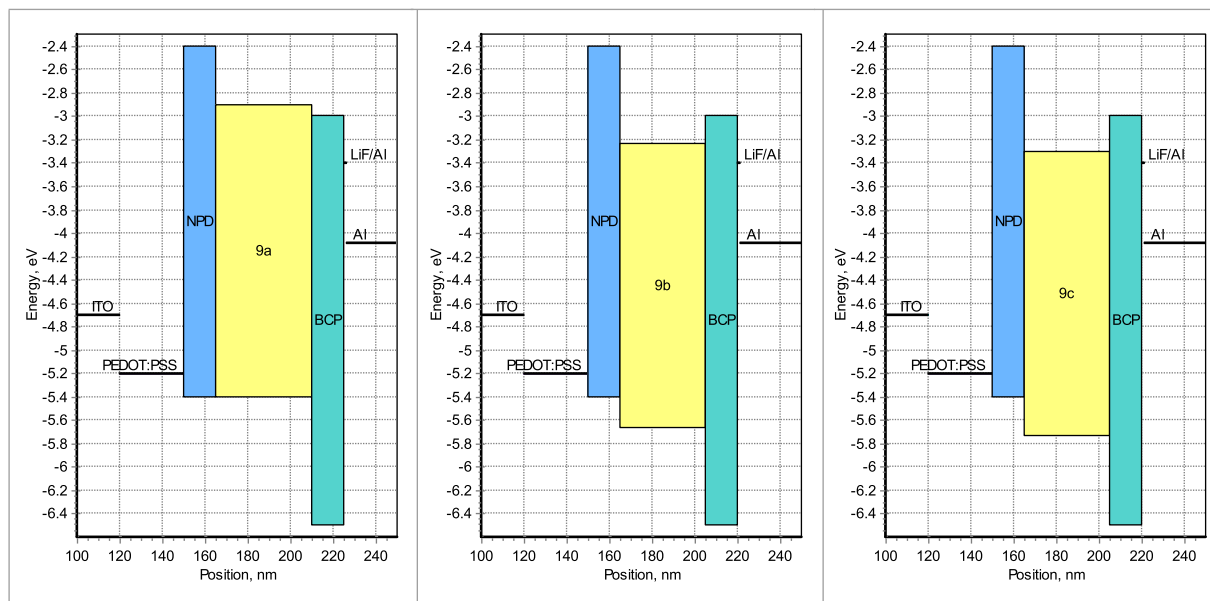


Fig. 6. OLED energy diagrams for devices based on **9a**, **9b**, and **9c**.

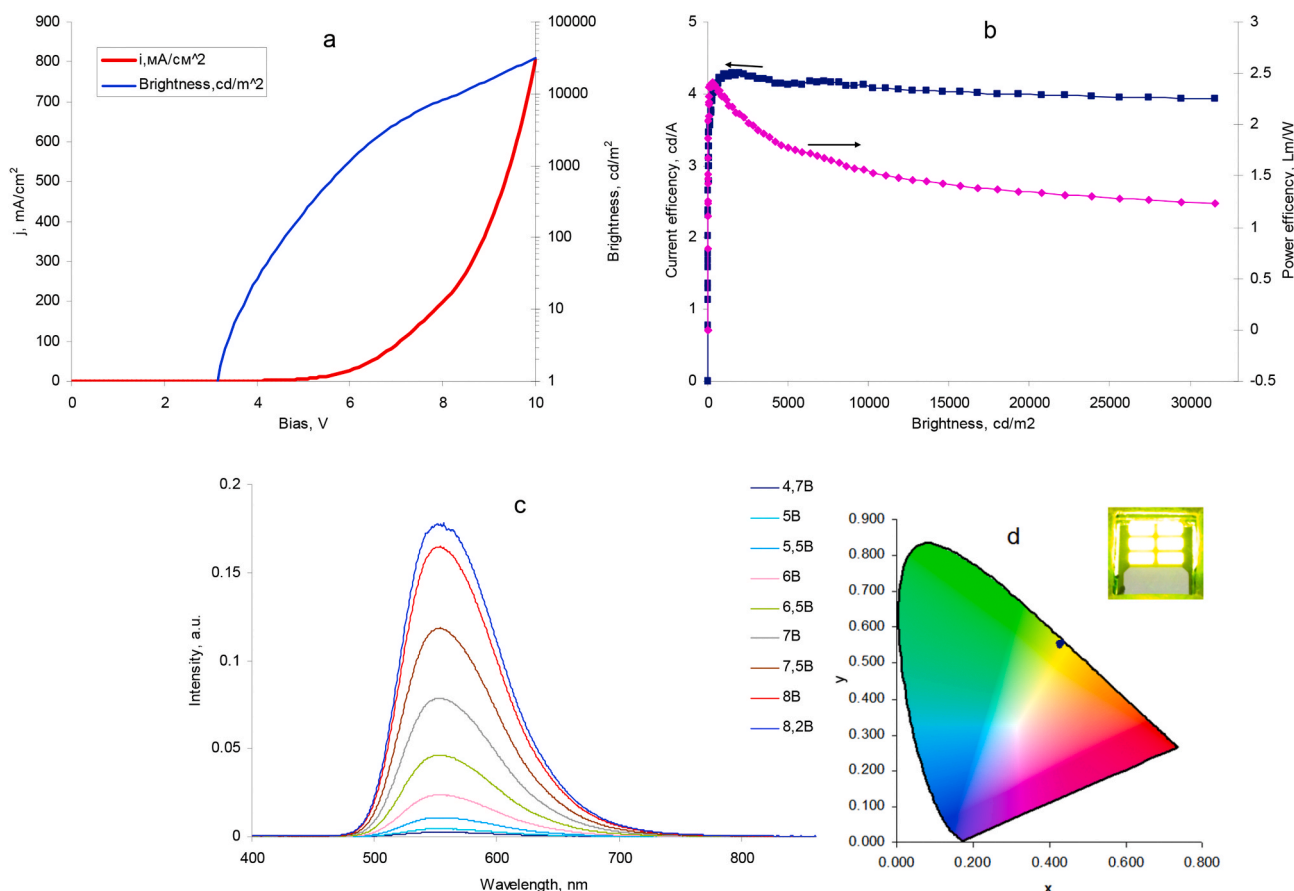


Fig. 7. Current-voltage and current-brightness characteristics (a), current and power efficiency (b), electroluminescent spectra at different voltages (c), and CIE1931 diagram (d) of OLED based on **9a**. The inset depicts the photo of this device with bright yellow emission.

structure, γ_{eh} is a factor showing the efficiency of electron-hole recombination (for well balanced structures is close to 100%), β_{ST} is the spin statistical limit (it results on the ratio of the probability of formation of singlet and triplet excitons at 1:3 and constitutes generally 25% for singlet emitters). According to the literature [55], it has been estimated that the internal quantum efficiency will achieve 6.3% with the obtained EQE of 1.26% for the device based on **9a** and the light output from the OLED structure on a glass substrate 20%. The approximately 63% of excitons will exist in the singlet state for **9a** at fluorescence quantum yield of 10% and a balance of electrons and holes 100% that significantly exceeding the spin statistics limit of 25%. For compounds **7a**, **7b**, **8a**, **8b**, and **9b**, the spin statistical limit of 25% has been also overcome and reached 27–44%. The portion of singlet excitons for **9c** has been less (16%) due to the rather high leakage currents that probably has been connected with the presence of a significant energy barrier for holes. Thus, we believe that further optimization of OLED devices based on these compounds will manage to improve efficiency for other devices in the future.

4. Conclusion

Based on the analysis of electrochemical photophysical characteristics it has been revealed that changing the structure of the 1,4-diazine-based molecules from the D-(π)-A type results in significantly improved optical and electrochemical properties due to the change of the effective conjugation length. The studied compounds were tested in OLEDs with a current efficiency up to 4.2 cd/A for a yellow non-doped device with a maximum electroluminescence intensity observed at 555 nm. The usage of the “hot excitons” mechanism improves the device performance leading to an OLED with an increased brightness up to

31565 cd/m². These characteristics make the quinoxaline derivative **9a** the best candidate for application in OLED devices.

Declaration of competing interest

The authors declare that they have no known competing financial interests or personal relationships that could have appeared to influence the work reported in this paper.

Acknowledgments

This work (synthetic part) was supported by the Russian Science Foundation (Project No. 19-13-00234). The photo- and electroluminescent study was supported by The Tomsk State University competitiveness improvement program under grant No. 8.2.22.2020. NMR experiments were carried out by using equipment of the Center for Joint Use «Spectroscopy and Analysis of Organic Compounds» at the Postovsky Institute of Organic Synthesis of the Ural Branch of the Russian Academy of Sciences.

Appendix A. Supplementary data

Supplementary data to this article can be found online at <https://doi.org/10.1016/j.dyepig.2020.109124>.

References

- [1] Muller CD, Falcou A, Reckefuss N, Rojahn M, Wiederhirn V, Rudati P, Frohne H, Nuyken O, Becker H, Meerholz K. Multi-colour organic light-emitting displays by solution processing. *Nature* 2003;421:829–33. <https://doi.org/10.1038/nature01390>.

- [2] Kulkarni AP, Tonzola CJ, Babel A, Jenekhe SA. Electron transport materials for organic light-emitting diodes. *Chem Mater* 2004;16:4556–73. <https://doi.org/10.1021/cm049473l>.
- [3] Zhou L, Yang L, Yu M, Jiang Y, Liu C-F, Lai W-Y, Huang W. Inkjet-printed small-molecule organic light-emitting diodes: halogen-free inks, printing optimization, and large-area patterning. *ACS Appl Mater Interfaces* 2017;9:40533–40. <https://doi.org/10.1021/acsami.7b13355>.
- [4] Pashaei B, Karimi S, Shahroosvand H, Abbasi P, Pilkington M, Bartolotta A, Fresta E, Fernandez-Cestau J, Costa RD, Bonaccorso F. Polypyridyl ligands as a versatile platform for solid-state light-emitting devices. *Chem Soc Rev* 2019;48:5033–139. <https://doi.org/10.1039/C8CS00075A>.
- [5] Buré F. Fundamental aspects of property tuning in push–pull molecules. *RSC Adv* 2014;4:58826–51. <https://doi.org/10.1039/C4RA11264D>.
- [6] Wei Q, Fei N, Islam A, Lei T, Hong L, Peng R, Fan X, Chen L, Gao P, Ge Z. Small-molecule emitters with high quantum efficiency: mechanisms, structures, and applications in OLED devices. *Adv. Optical Mater.* 2018;6:1800512. <https://doi.org/10.1002/adom.201800512>.
- [7] Zhao X, Chaudhry ST, Mei J. Heterocyclic building blocks for organic semiconductors. *Adv Heterocycl Chem* 2017;121:133–71. <https://doi.org/10.1016/BS.AIHCH.2016.04.009>.
- [8] Xu X, Yu G, Chen S, Di C, Liu Y. Synthesis and characterization of a quinoxaline compound containing polyphenylphenyl and strong electron-accepting groups, and its multiple applications in electroluminescent devices. *J Mater Chem* 2008;18:299–305. <https://doi.org/10.1039/B710139B>.
- [9] Yuan J, Ouyang J, Cimrová V, Leclerc M, Najari A, Zou Y. Development of quinoxaline based polymers for photovoltaic applications. *J Mater Chem C* 2017;5:1858–79. <https://doi.org/10.1039/C6TC05381E>.
- [10] Meti P, Park H-H, Gong Y-D. Recent developments in pyrazine functionalized π -conjugated materials for optoelectronic applications. *J Mater Chem C* 2020;8:352–79. <https://doi.org/10.1039/C9TC05014K>.
- [11] Nosova EV, Achelle S, Lipunova GN, Charushin VN, Chupakhin ON. Functionalized benzazines as luminescent materials and components for optoelectronics. *Russ Chem Rev* 2019;88:1128–78. <https://doi.org/10.1070/RCR4887>.
- [12] Achelle S, Baudequin C, Plé N. Luminescent materials incorporating pyrazine or quinoxaline moieties. *Dyes Pigments* 2013;98:575–600. <https://doi.org/10.1016/j.dyepig.2013.03.030>.
- [13] Lin S-L, Chan L-H, Lee R-H, Yen M-Y, Kuo W-J, Chen C-T, Jeng R-J. Highly efficient carbazole- π -dimesitylborane bipolar fluorophores for nondoped blue organic light-emitting diodes. *Adv. Mater.* 2008;20:3947–52. <https://doi.org/10.1002/adma.200801023>.
- [14] Kwak J, Lyu Y-Y, Lee H, Choi B, Char K, Lee C. New carbazole-based host material for low-voltage and highly efficient red phosphorescent organic light-emitting diodes. *J Mater Chem* 2012;22:6351–5. <https://doi.org/10.1039/C2JM15138C>.
- [15] Mortimer RJ. Electrochromic materials. *Chem Soc Rev* 1997;26:147–56. <https://doi.org/10.1039/CS9972600147>.
- [16] Hagfeldt A, Boschloo G, Kloo L, Pettersson H. Dye-sensitized solar cells. *Chem Rev* 2010;110:6595–6663. <https://doi.org/10.1021/cr900356p>.
- [17] Sakong C, Kim HJ, Kim SH, Namgoong JW, Park JH, Ryu J-H, Kim B, Ko MJ, Kim J. Synthesis and applications of new triphenylamine dyes with donor–donor–(bridge)–acceptor structure for organic dye-sensitized solar cells. *New J Chem* 2012;36:2025–32. <https://doi.org/10.1039/C2NJ40374A>.
- [18] Lin Y, Li Y, Zhan X. Small molecule semiconductors for high-efficiency organic photovoltaics. *Chem Soc Rev* 2012;41:4245–72. <https://doi.org/10.1039/C2CS15313K>.
- [19] Mishra A, Bäuerle P. Small molecule organic semiconductors on the move: promises for future solar energy technology. *Angew Chem Int Ed* 2012;51:2020–67. <https://doi.org/10.1002/anie.201102326>.
- [20] Kanaparthi RK, Kandhdi J, Giribabu L. Metal-free organic dyes for dye-sensitized solar cells: recent advances. *Tetrahedron* 2012;68:8383–93. <https://doi.org/10.1016/j.tet.2012.06.064>.
- [21] Verbitskiy EV, Achelle S, Bureš F, le Poul P, Barsella A, Kvashnin YA, Rusinov GL, Robin-le Guen F, Chupakhin ON, Charushin VN. Synthesis, photophysical and nonlinear optical properties of [1,2,5]oxadiazolo[3,4-*b*]pyrazine-based linear push-pull systems. *J Photochem Photobiol Chem* 2021;404:112900. <https://doi.org/10.1016/j.jphotochem.2020.112900>.
- [22] Verbitskiy EV, Cheprakova EM, Subbotina JO, Schepochkin AV, Slepukhin PA, Rusinov GL, Charushin VN, Chupakhin ON, Makarova NI, Metelitsa AV, Synthesis VI Minkin. Spectral and electrochemical properties of pyrimidine-containing dyes as photosensitizers for dye-sensitized solar cells. *Dyes Pigments* 2014;100:201–14. <https://doi.org/10.1016/j.dyepig.2013.09.006>.
- [23] Verbitskiy EV, Schepochkin AV, Makarova NI, Dorogan IV, Metelitsa AV, Minkin VI, Kozuyukhin SA, Emets VV, Grindberg VA, Chupakhin ON, Rusinov GL, Charushin VN. Synthesis, photophysical and redox properties of the D– π –A type pyrimidine dyes bearing the 9-phenyl-9*H*-carbazole moiety. *J Fluoresc* 2015;25:763–75. <https://doi.org/10.1007/s10895-015-1565-6>.
- [24] Song Y, Di C, Xu Wei, Liu Y, Zhang D, Zhu D. New semiconductors based on triphenylamine with macrocyclic architecture: synthesis, properties and applications in OFETs. *J Mater Chem* 2007;17:4483–91. <https://doi.org/10.1039/B708887F>.
- [25] Allard S, Forster M, Souharce B, Thiem H, Scherf U. Organic semiconductors for solution-processable field-effect transistors (OFETs). *Angew Chem Int Ed* 2008;47:4070–98. <https://doi.org/10.1002/anie.200701920>.
- [26] Wang C, Dong H, Hu W, Liu Y, Zhu D. Semiconducting π -conjugated systems in field-effect transistors: a material odyssey of organic electronics. *Chem Rev* 2012;112:2208–67. <https://doi.org/10.1021/cr100380z>.
- [27] Li Y, Liu J-Y, Zhao Y-D, Cao Y-C. Recent advancements of high efficient donor–acceptor type blue small molecule applied for OLEDs. *Mater Today* 2017;20:258–66. <https://doi.org/10.1016/j.mattod.2016.12.003>.
- [28] Ledwon P. Recent advances of donor-acceptor type carbazole-based molecules for light emitting applications. *Org Electron* 2019;75:105422. <https://doi.org/10.1016/j.orgel.2019.105422>.
- [29] Blanchard P, Malacrida C, Cabanetos C, Roncali J, Ludwigs S. Triphenylamine and some of its derivatives as versatile building blocks for organic electronic applications. *Polym Int* 2019;68:589–606. <https://doi.org/10.1002/pi.5695>.
- [30] Roncali J. Synthetic principles for bandgap control in linear π -conjugated systems. *Chem Rev* 1997;97:173–206. <https://doi.org/10.1021/cr950257t>.
- [31] Turkoglu G, Cinar ME, Ozturk T. Thiophene-based organic semiconductors. *Top Curr Chem* 2017;375:84. <https://doi.org/10.1007/s41061-017-0174-z>.
- [32] Rangisetty JB, Gupta CNVHB, Prasad AL, Srinivas P, Sridhar N, Parimoo P, Veeranjanyulu A. Synthesis of new arylaminoquinoxalines and their antimalarial activity in mice. *J Pharm Pharmacol* 2001;53:1409–13. <https://doi.org/10.1211/002235701177765>.
- [33] Verbitskiy EV, Kvashnin YA, Baranova AA, Khokhlov KO, Chuvashov RD, Schapov IE, Yakovleva YA, Zhilina EF, Schepochkin AV, Makarova NI, Vetrova EV, Metelitsa AV, Rusinov GL, Chupakhin ON, Synthesis V N Charushin. Solvatochromism and sensitivity towards nitroaromatic compounds and aliphatic amines of 1,4-diazine-based dyes bearing triphenylamine donor group. *Dyes Pigments* 2020;178:108344. <https://doi.org/10.1016/j.dyepig.2020.108344>.
- [34] de Mello JC, Wittmann HF, Friend RH. An improved experimental determination of external photoluminescence quantum efficiency. *Adv. Mater.* 1997;9:230–2. <https://doi.org/10.1002/adma.19970090308>.
- [35] Cardona CM, Li W, Kaifer AE, Stockdale D, Bazan GC. Electrochemical considerations for determining absolute frontier orbital energy levels of conjugated polymers for solar cell applications. *Adv. Mater.* 2011;23:2367–71. <https://doi.org/10.1002/adma.201004554>.
- [36] Casida ME. Time-dependent density functional response theory for molecules. In: *Recent advances. In density functional methods: (Part I)*; 1995. p. 155–92. https://doi.org/10.1142/9789812830586_0005.
- [37] Adamo C, Barone V. Toward reliable density functional methods without adjustable parameters: the PBE0 model. *J Chem Phys* 1999;110:6158–70. <https://doi.org/10.1063/1.478522>.
- [38] Neese F. The ORCA program system. *Wiley Interdiscip Rev. Comput. Mol. Sci.* 2012;2:73–8. <https://doi.org/10.1002/wcms.81>.
- [39] Andrienko GA. Chemcraft. Graphical software for visualization of quantum chemistry computations. <https://www.chemcraftprog.com/>; 2010.
- [40] Valiev RR, Minaev BF, Gadirov RM, Nikonova EN, Solodova TA, Nikonov SY, Bushuev MB, Kopylova TN. Electroluminescence of halogen complexes with monovalent copper: OLED devices and DFT modeling. *Russ Phys J* 2016;58:1205–11. <https://doi.org/10.1007/s11182-016-0633-y>.
- [41] Wang P, Yang Z, Wang Z, Xu C, Huang L, Wang S, Zhang H, Lei A. Electrochemical arylation of electron-deficient arenes through reductive activation. *Angew Chem Int Ed* 2019;58:15747–51. <https://doi.org/10.1002/anie.201909600>.
- [42] Rao X, Liu C, Qiu J, Jin Z. A highly efficient and aerobic protocol for the synthesis of *N*-heteroarylsubstituted 9-arylcarbazolyl derivatives via a palladium-catalyzed ligand-free Suzuki reaction. *Org Biomol Chem* 2012;10:7875–83. <https://doi.org/10.1039/C2OB26119G>.
- [43] Lippert E, Lüder W, Moll F. Polarisations- und relaxations-effekte in der Temperaturabhängigkeit von Absorptions- und fluoreszenzspektren aromatischer verbindungen in polaren Lösungsmitteln. *Spectrochim Acta* 1959;15:858–69. [https://doi.org/10.1016/S0371-1951\(59\)80383-0](https://doi.org/10.1016/S0371-1951(59)80383-0).
- [44] Ishchenko AA, Kulich AV, Bondarev SL, Knyukshto VN, Turban AA. Thermochromism and thermofluorochromism of merocyanines with a positive solvatochromism. *Optic Spectrosc* 2006;101:90–7. <https://doi.org/10.1134/S0030400X06070162>.
- [45] Zhang Q, Li B, Huang S, Nomura H, Tanaka H, Adachi C. Efficient blue organic light-emitting diodes employing thermally activated delayed fluorescence. *Nat Photon* 2014;8:326–32. <https://doi.org/10.1038/nphoton.2014.12>.
- [46] Pan Y, Huang J, Li W, Gao Y, Wang Z, Yu D, Yang B, Ma Y. Theoretical investigation of high-efficiency organic electroluminescent material: HLCT state and hot exciton process. *RSC Adv* 2017;7:19576–83. <https://doi.org/10.1039/C7RA01270E>.
- [47] Kondakov DY, Pawlik TD, Hatwar TK, Spindler JP. Triplet annihilation exceeding spin statistical limit in highly efficient fluorescent organic light-emitting diodes. *J Appl Phys* 2009;106:124510. <https://doi.org/10.1063/1.3273407>.
- [48] Dias FB, Bourdakos KN, Jankus V, Moss KC, Kamtekar KT, Bhalla V, Santos J, Bryce MR, Monkman AP. Triplet harvesting with 100% efficiency by way of thermally activated delayed fluorescence in charge transfer OLED emitters. *Adv. Mater.* 2013;25:3707–14. <https://doi.org/10.1002/adma.201300753>.
- [49] Liu J, Li Z, Hu T, Wei X, Wang R, Hu X, Liu Y, Yi Y, Yamada-Takamura Y, Wang Y, Wang P. Experimental evidence for “hot exciton” thermally activated delayed fluorescence emitters. *Adv. Optical Mater.* 2019;7:1801190. <https://doi.org/10.1002/adom.201801190>.
- [50] B Dias F, Penfold TJ, Monkman AP. Photophysics of thermally activated delayed fluorescence molecules. *Methods Appl Fluoresc* 2017;5:012001. <https://doi.org/10.1088/2050-6120/aa537e>.
- [51] Permogorov S. Hot excitons in semiconductors. *Phys Status Solidi B* 1975;68:9–42. <https://doi.org/10.1002/pssb.2220680102>.
- [52] Lee H, Kwak J, Kang CM, Lyu YY, Char K, Lee C. Trap-level-engineered common red layer for fabricating red, green, and blue subpixels of full-color organic light-emitting diode displays. *Optic Express* 2015;23:11424–35. <https://doi.org/10.1364/OE.23.11424>.

- [53] Toyoshima S, Kuwabara K, Sakurai T, Taima T, Saito K, Kato H, Akimoto K. Electronic structure of bathocuproine on metal studied by ultraviolet photoemission spectroscopy. *Jpn J Appl Phys* 2007;46:2692. <https://doi.org/10.1143/JJAP.46.2692>.
- [54] Konyshv YV, Gadirov RM, Valiev RR, Odod AV, Degtyarenko KM, Krasnikova SS, Yakushchenko IK, Kopylova TN. *Russ Phys J* 2019;62:140–6. <https://doi.org/10.1007/s11182-019-01694-z>.
- [55] Li W, Pan Y, Xiao R, Peng Q, Zhang S, Ma D, Li F, Shen F, Wang Y, Yang B, Ma Y. Employing ~100% excitons in OLEDs by utilizing a fluorescent molecule with hybridized local and charge-transfer excited state. *Adv Funct Mater* 2014;24:1609–14. <https://doi.org/10.1002/adfm.201301750>.